This is to certify that the

thesis entitled

A Compensated Actuator for
an Acoustic Duct

presented by

Charles Birdsong

has been accepted towards fulfillment
of the requirements for

Masters ____ degree in __Mechanical__ Engineering

Major professor

Date__ 12/10/96 _____

PLACE IN RETURN BOX to remove this checkout from your record.
TO AVOID FINES return on or before date due.

DATE DUE	DATE DUE	DATE DUE
NOV 02 3 2002		

MSU Is An Affirmative Action/Equal Opportunity Institution

A COMPENSATED ACTUATOR
FOR AN ACOUSTIC DUCT

By

Charles Birdsong

A THESIS

Submitted to
Michigan State University
in partial fulfillment of the requirements
for the degree of

MASTER OF SCIENCE

Department of Mechanical Engineering

1996

ABSTRACT

A COMPENSATED ACTUATOR
FOR AN ACOUSTIC DUCT

By

Charles Birdsong

Audio speakers are commonly used as acoustic actuators for noise control applications. Recent developments in the use of compensated dual-coil speakers have improved the performance of these acoustic actuators. However, the performance of these speakers depends on the application. When they are applied in systems with strong coupling between the plant and the actuator such as an acoustic duct, the velocity sensor used in previous work must be improved.

This study considers the application of a compensated speaker as an actuator in noise control of an acoustic duct. The speaker dynamics and the acoustic duct dynamics are first modeled separately. The two systems are then coupled, and the resulting system is modeled. A velocity sensor is developed and used in feed-back compensation. The resulting speaker system behaves as an ideal actuator with minimal magnitude and phase variation over a $0 - 200$ Hz bandwidth. These conclusions are verified through experimental results.

This study is important in the overall area of acoustic actuators and active noise control. The actuator developed here will significantly aid in the goal of active noise control in an acoustic duct.

DEDICATION

I dedicate this work to my loving wife Bernadette whose support and understanding have given strength.

ACKNOWLEDGMENTS

TABLE OF CONTENTS

LIST OF TABLES

LIST OF FIGURES

Page

1. INTRODUCTION

Active noise control is an expanding field in the automotive and aircraft industries. Commercial products are currently available to create quiet interior spaces [Bradley 1995, Warner 1995]. These systems use passive and active controls to treat unwanted noise. Passive control consists of applying dampening material to treat high frequency noise. Dampening material must be of the same physical dimension as the wavelength of the sound wave to be effective [General Motors 1994]. Below 200 Hz the wave length in air is approximately 0.26 m or longer. This would require an unrealistic amount of dampening material approximately one quarter of a meter thick for effective passive noise control. For low frequency noise, active controls methods can be used. Active control relies on a combination of sensors, a controller, and actuators to treat noise in the system (plant). Figure 1.1 shows a typical active noise control system where a microphone is used as a sensor and an audio speaker is used as an acoustic actuator to treat noise in an interior space.
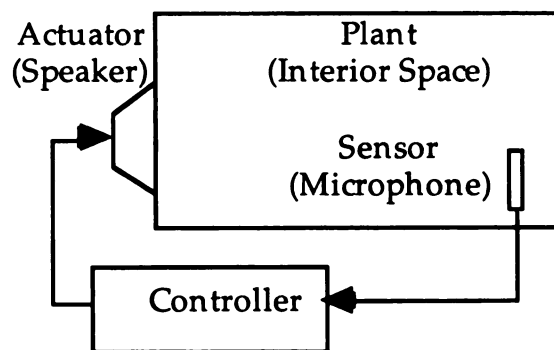
Figure 1.1. Typical Noise Control System

One system that has received much attention in this field is the acoustic duct, which consists of a long, hard walled enclosure. Hull showed that the resonances excited by a noise source in an acoustic duct can be attenuated using feedback active noise control [Hull 1993]. Attempts at wide band noise control were hindered by actuator dynamics that caused the measured control input to deviate from the desired control.

Gogate proposed a strategy for eliminating the effects of speaker dynamics through feed-back compensation [Radcliffe et al. 1996]. The original design did not include the effects of the coupled dynamics through the interaction of the plant pressure and the actuator. Figure 1.2 shows the speaker face velocity to primary coil voltage frequency response of the original compensator with two cases: the dashed line represents the response of the speaker in free-air, and the solid line represents the response when the speaker is coupled with an acoustic duct. In free-air there is little magnitude and phase variation from 0 - 200 Hz. When the speaker is coupled with the acoustic duct, there are large magnitude and phase variations exhibited at the resonance frequencies of the duct. The original compensator fails to eliminate the dynamics associated with the duct.
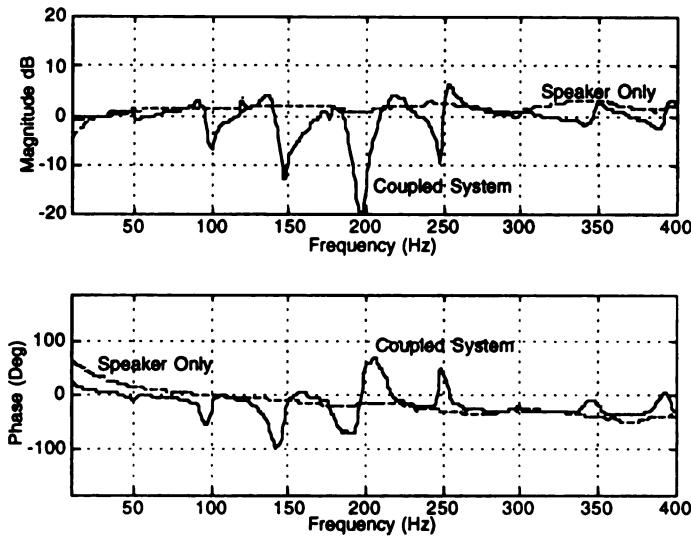
Figure 1.2. Speaker Face Velocity to Primary Coil Voltage
Using Original Compensator

This study presents an acoustic actuator that compensates for both

actuator and plant dynamics. The acoustic duct is presented as a plant in

order to demonstrate the robustness of the system to a plant with strong

coupling with the actuator through pressure interaction. A model of a dual

voice-coil speaker is first presented, and a velocity sensor is developed. It is

shown that the speaker dynamics can be eliminated through feed-back

compensation. A model of an acoustic duct is presented next, which predicts

the pressure response due to a velocity input. Finally, the two systems are

coupled, and it is shown that the speaker compensation minimizes both the

speaker and the acoustic duct dynamics through feed-back compensation.

The results in every stage of the modeling and analysis are verified through

experimental testing, and model results are presented together with

experimental results. Figure 1.3 shows the experimental setup used to verify

the model results.
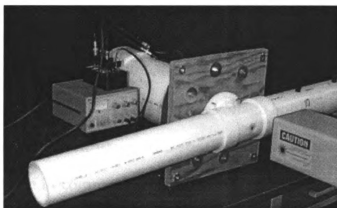
Figure 1.3. Acoustic Duct and Compensated Actuator Setup

The work presented here provides a method for creating an ideal acoustic actuator for systems that include strong plant and actuator coupling and brings the goal of active noise control of systems such as the acoustic duct one step closer.

2. ACOUSTIC ACTUATOR SPEAKER MODEL

Audio speakers are commonly used as acoustic actuators in noise control systems. They are beneficial because a small voltage applied to a speaker can generate a strong control effort. Audio speakers are relatively inexpensive and widely available in commercial sizes and models. Speakers have the disadvantage that the response of a speaker can be strongly affected by both the dynamics associated with the free-air resonance of the speaker and the dynamics of the system it is driving. An ideal actuator will have a pure gain over the required bandwidth. When a speaker is affected by dynamics, it can exhibit significant magnitude and phase variations limiting its performance. If a speaker is to be used as an acoustic actuator, these effects must be minimized.

One method of minimizing magnitude and phase variations is to apply feedback compensation to the speaker. If the speaker response can be measured, then the signal can be applied to a feedback controller, the response can be driven to the desired output, and the magnitude and phase variation can be reduced. An accurate speaker face velocity sensor is therefore required.

The development of a speaker, velocity sensor model and the system transfer functions follows. The model is then used to develop a feedback compensation strategy. Finally, the model is verified through experimental testing.

Identification and Modeling of Speaker Dynamics

One variety of speaker named the "dual voice-coil" speaker has certain characteristics that make it ideal for use as an acoustic actuator [Radcliffe et al. 1996]. The dual voice-coil speaker has 2 independent wire coils intertwined and wrapped around a bobbin which is allowed to slide over a permanent magnet. This configuration is shown in Figure 2.1.
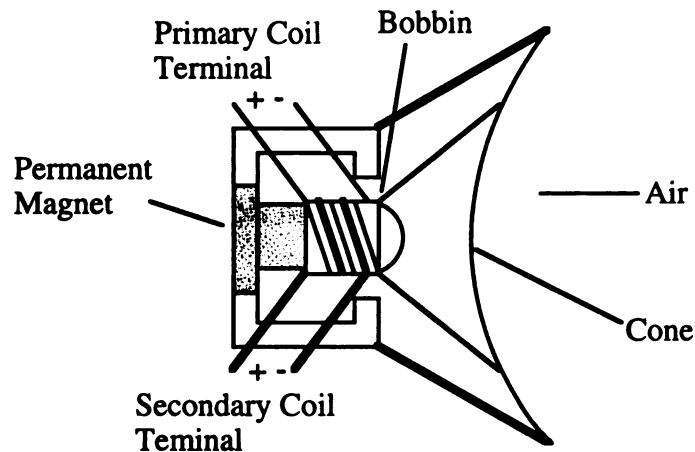
Figure 2.1. Dual Voice-Coil Speaker Diagram

The electromagnetic speaker is a system that involves mechanical, electrical, and magnetic energy domains. This class of problem is well suited to modeling using the Bond Graph technique [Karnopp et al 1990]. Figure 2.2 shows the bond graph diagram of the dual voice-coil speaker system [Radcliffe et al. 1996]. The previously available bond graph model is used here with the addition of one 'R' element which represents a current sensing resistor. New velocity transfer functions are derived from the bond graph model and used in the speaker feedback control system.
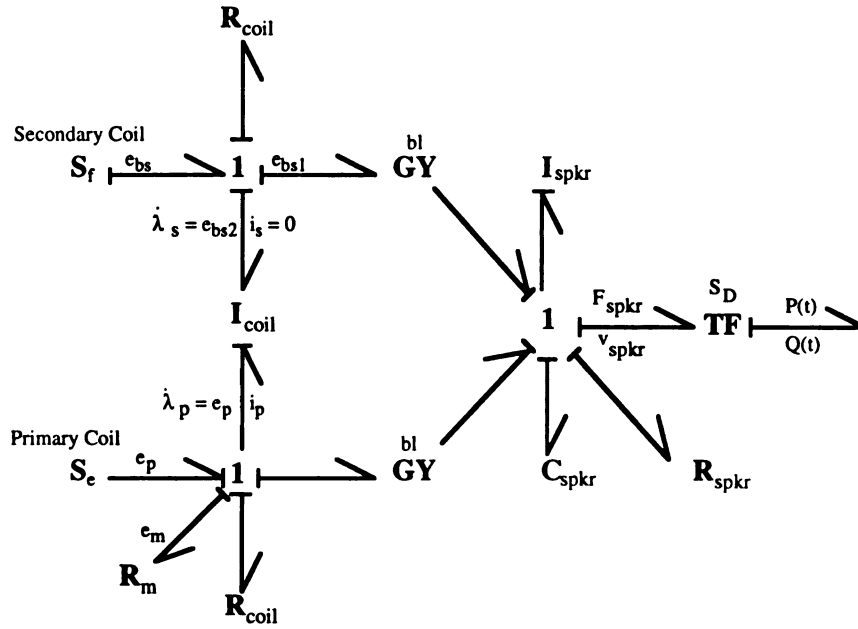
Figure 2.2. Bond Graph of Dual Voice-Coil Speaker System

The Bond Graph arrows represent power flow from the electrical voltage, S_e, applied at the primary coil through the model's elements. Power is dissipated in resistive elements R_{coil}, R_m and R_{spkr} and transformed both from electrical to mechanical power in the 'GY' element and from mechanical to acoustic power in the 'TF' element. Power is stored as kinetic energy in the 'I' elements and as potential energy in the 'C' elements. The open circuit on the secondary coil is represented by a secondary coil current (i_s =0) imposed by the source of flow, S_f.

The energy variables in the bond graph model include coil flux linkages, λ_p and λ_s; speaker cone displacement, x_{spkr}; and speaker cone velocity, v_{spkr}. A linear approximation is used to relate the flux linkages, λ_p and λ_s, of the multiport I_{coil} field to the port currents, i_p and i_s, in the primary and secondary coils.

The state equations for the speaker model can be written from the bond graph in state space form by choosing energy variables as state variables and appropriate input and output variables. A complete derivation is given in Appendix A.

$$\dot{x}(t) = A_{spkr}x(t) + B_{spkr}u_{spkr}(t) \tag{2.1}$$

where

$$A_{spkr} = \begin{bmatrix} 0 & 1 & 0 \\ \dfrac{-1}{C_{spkr}I_{spkr}} & \dfrac{-R_{spkr}}{I_{spkr}} & \dfrac{bl}{(I_{spkr}I_{coil})} \\ 0 & -bl & \dfrac{-(R_{coil}+R_m)}{I_{coil}} \end{bmatrix}, \quad B_{spkr} = \begin{bmatrix} 0 & 0 \\ 0 & \dfrac{-S_D}{I_{spkr}} \\ 1 & 0 \end{bmatrix} \tag{2.2}$$

The state variables are $x_{spkr} = \begin{pmatrix} x_{spkr} \\ v_{spkr} \\ \lambda_p \end{pmatrix}$, speaker face displacement, x_{spkr}; speaker face velocity, v_{spkr}; and primary coil flux, λ_p. The input variables are

$u_{spkr} = \begin{pmatrix} e_p \\ P \end{pmatrix}$; speaker primary coil voltage, e_p; and speaker face pressure, P.

The output equations for the speaker model can be arranged in state equation format as

$$y_{spkr}(t) = C_{spkr}x_{spkr}(t) + D_{spkr}u_{spkr}(t) \tag{2.3}$$

where the output variables, $y_{spkr} = \begin{pmatrix} e_{bs} \\ i_p \\ v_{spkr} \end{pmatrix}$ are speaker secondary coil voltage,

$e_{bs}(t)$; speaker drive current in the primary coil, $i_p(t)$; and speaker face velocity, v_{spkr}. The output matrices are

$$C_{spkr} = \begin{bmatrix} 0 & bl\left(1 - \dfrac{M_{coil}}{I_{coil}}\right) & -\dfrac{M_{coil}}{I_{coil}^2}(R_{coil} + R_m) \\ 0 & 0 & \dfrac{1}{I_{coil}} \\ 0 & 1 & 0 \end{bmatrix}, \quad D_{spkr} = \begin{bmatrix} \dfrac{M_c}{I_c} & 0 \\ 0 & 0 \\ 0 & 0 \end{bmatrix} \quad (2.4)$$

Equations (2.1) and (2.3) define the model of a dual voice-coil speaker. The speaker parameters necessary to define the model are the mechanical inertia of speaker, I_{spkr}; mechanical compliance of speaker, C_{spkr}; viscous friction of speaker, R_{spkr}; electromagnetic coupling factor, bl; speaker coil resistance, R_{coil}; speaker coil inductance, I_{coil}, mutual inductance, M_{coil}; and the equivalent speaker area, S_D. With the exception of mutual inductance, M_{coil}, these electrical and mechanical parameters are defined in IEEE standard 219-1975 [IEEE Standard 219-1975] for loudspeaker measurements.

Speaker Model Transfer Functions

The transfer function matrix can be determined from (2.1) and (2.3). The speaker model includes two inputs and three outputs, resulting in a transfer function matrix of dimension 3x2. The steady-state output of the system is given by [Rough, 1996]

$$Y(s) = \left[C(sI - A)^{-1} B + D \right] U(s) \tag{2.5}$$

where A is the state matrix; B is the input matrix; C is the output matrix; D is the direct feed-through matrix; 'sI' is the Laplace variable multiplied by an identity matrix, U(s); and Y(s) is are the input and output vectors in the Laplace domain.

The transfer function matrix is defined by

$$G(s) = C(sI - A)^{-1} B + D \tag{2.6}$$

Substituting the values of A, B and C, inverting sI-A and multiplying the matrices yields

$$\begin{pmatrix} e_{bs}(s) \\ i_p(s) \\ v_{spkr}(s) \end{pmatrix} = \begin{bmatrix} G_{ebs/ep} & G_{ebs/P} \\ G_{ip/ep} & G_{ip/P} \\ G_{vspkr/ep} & G_{vspkr/P} \end{bmatrix} \begin{pmatrix} e_p(s) \\ P(s) \end{pmatrix} \tag{2.7}$$

where each element in the transfer function matrix G(s) is given by

$$G_{ebs/ep} = \left[(C_{spkr} I_{spkr} M_{coil}) s^3 + (C_{spkr} R_{spkr} M_{coil}) s^2 + (bl^2 C_{spkr} + M_{coil}) s \right] \Big/ G_{den} \tag{2.8}$$

$$G_{ip/ep} = \left[(C_{spkr} I_{spkr}) s^2 + (C_{spkr} R_{spkr}) s + 1 \right] \Big/ G_{den} \tag{2.9}$$

$$G_{vspkr/ep} = \left[(bl\, C_{spkr}) s \right] \Big/ G_{den} \tag{2.10}$$

$$G_{ebs/P} = \left[-bl\, C_{spkr} S_D\left[(I_{coil} - M_{coil})s^2 + R_{coil}s\right]\right] \bigg/ G_{den} \qquad (2.11)$$

$$G_{ip/P} = \left[(bl\, S_D C_{spkr})s\right] \bigg/ G_{den} \qquad (2.12)$$

$$G_{vspkr/P} = \left[-S_D C_{spkr}\left[I_{coil}s^2 + R_{coil}s\right]\right] \bigg/ G_{den} \qquad (2.13)$$

and the denominator of the G(s) matrix is given as

$$G_{den} = (C_{spkr}I_{spkr}I_{coil})s^3 + (C_{spkr}I_{spkr}R_{coil} + C_{spkr}I_{coil}R_{spkr})s^2 + $$
$$(bl^2 C_{spkr} + I_{coil} + C_{spkr}R_{coil}R_{spkr})s + R_{coil} \qquad (2.14)$$

Equations (2.10) and (2.13) are new and important results not used in previous work. All of the speaker model transfer function equations will be useful when designing a velocity sensor for the speaker and when modeling the speaker coupled with the acoustic duct.

Velocity Feedback Compensation of Speaker

The velocity of the speaker, v_{spkr}, is strongly affected by the dynamics of the speaker and the pressure input, P. These effects will combine to create magnitude and phase variations in the primary coil voltage to speaker velocity response. One method of eliminating these unwanted effects is to apply a proportional feedback controller as shown in Figure 2.3. The transfer function for this system is given by (2.15), where K_p is the proportional gain and H(s) is a velocity sensor. If the sensor transfer function is a real constant,

k, over the controller bandwidth, then the closed loop transfer function, T(s), will approach a constant, 1/k with zero phase. This compensation forces the speaker cone velocity to accurately follow the desired velocity input. The result is independent of the speaker dynamics and the input pressure provided that the sensor has a constant transfer function over the controller bandwidth.
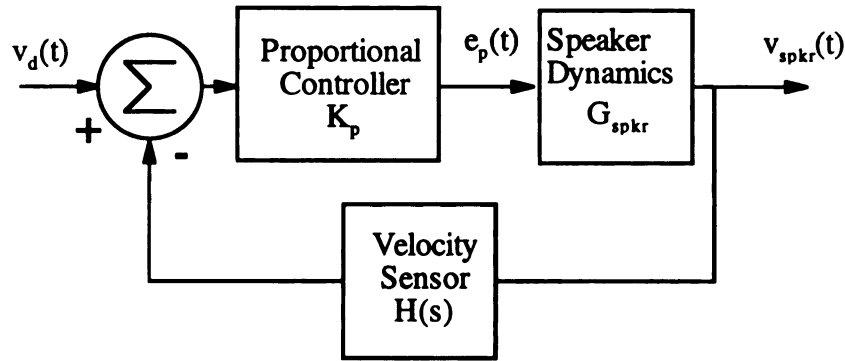
Figure 2.3. Proportional Feedback Controller

$$T_{spkr}(s) = \frac{V_{spkr}(s)}{V_d(s)} = \frac{K_p G_{spkr}(s)}{1 + K_p G_{spkr}(s)H(s)} \qquad (2.15)$$

As K_p is increased, the transfer approaches 1/H(s) and the magnitude and phase variation approaches zero. This approach assumes that the velocity of the speaker face can be measured. A speaker velocity sensor is therefore needed which accurately predicts the speaker velocity in the presence of speaker and plant dynamics.

The relation between the speaker velocity and the two other measurable outputs (the secondary coil voltage, e_{bs} and the primary coil current, i_p) is

given in (2.7). The speaker velocity, V_{spkr} can be solved for in terms of E_{bs} and I_p yielding,

$$V_{spkr}(s) = H_{bs}E_{bs}(s) - H_p(s)I_p(s) \tag{2.16}$$

where $H_{bs} = 1/bl$ and $H_p(s) = sM_{coil}/bl$.

The secondary coil voltage, E_{bs}, can be measured directly from the speaker coil; the primary coil current, I_p, can be determined from the voltage across the resistor, R_m; and H_{bs} is a pure gain $(1/bl)$. The term $H_p(s)$ is a differentiator transfer function because it contains an 's' in the numerator. Such a transfer function cannot be realized exactly, but an approximation $\hat{H}_p(s)$ can be used where

$$\hat{H}_p(s) = \frac{M_{coil}}{bl}\left(\frac{s}{s + p_1}\right) \tag{2.17}$$

where p_1 is a pole location selected such that $\hat{H}_p(s)$ approximates $H_p(s)$ over the controller bandwidth.

Feedback compensation can now be implemented using the signal from the velocity sensor to compute the error between the desired velocity and the sensor velocity and a proportional controller to drive the speaker velocity to the desired velocity. It should be noted that the development of the velocity sensor did not assume that the pressure at the speaker face was constant, as in previous work. This new velocity sensor includes the effects of pressure as an

input to the system. As a result, the closed-loop system minimizes magnitude and phase variations from not only the speaker dynamics (as in previous work) but in addition, the dynamics associated with the acoustic system, coupled through the pressure interaction with the speaker are minimized as well. This improvement over the previous velocity sensor is essential for the speaker to perform as an ideal actuator in a coupled system such as the acoustic duct.

Speaker Model Verification

The system model was verified through experimental testing. The open-loop speaker system was assembled, and the system response was compared to the model. A velocity sensor was then created and tested; and finally, the closed-loop system response was compared to the model. Figure 2.4 shows the dual voice-coil speaker in an enclosure with the velocity transducer.
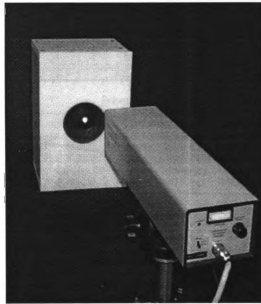
Figure 2.4. Dual Voice-Coil Speaker and Velocity Transducer

Speaker Dynamics

A 6-inch dual voice-coil speaker was mounted in an enclosure and the physical parameters of the speaker system were determined [Radcliffe 1992].

The speaker velocity to voltage transfer function was computed (2.7) with the speaker face pressure, P set equal to zero. This assumption was based on the fact that when the speaker operates in free air, the pressure variation on the speaker face is negligible. The speaker velocity to voltage transfer function was then measured experimentally with a Hewlett Packard Signal Analyzer 35660A. The speaker face velocity was measured with a Bruel & Kjaer Laser Doppler Velocity-Transducer Set Type 3544. Figure 2.5 shows the close correlation with the experimental and model results. The solid line represents the model, and the dotted line indicates the experimental response.
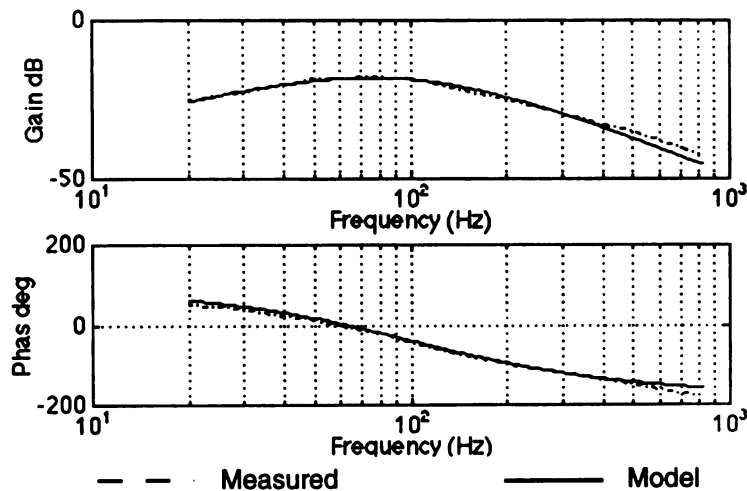
Figure 2.5. Comparison of Theoretical and Experimental Speaker Velocity Response

The speaker velocity response is affected by the dynamics of the free-air resonance. There are approximately 20 dB and 180 degrees in magnitude and phase variation from 1 - 200 Hz. While (2.7) shows that the transfer function is third order, Figure 2.5 suggests that it can be modeled by a second order system below approximately 200 Hz. The effective natural frequency of the system can be calculated as

$$f_{neff} = \sqrt{\frac{1}{C_{spkr}I_{spkr}}} = 62 Hz \tag{2.18}$$

which matches the resonance frequency in Figure 2.5. At frequencies above 200 Hz, the response deviates from the 2nd order response due to inductance effects. An ideal actuator will behave as a pure gain over a given band-width. These results show that the speaker is an ineffective actuator when operated in open-loop.

Velocity Sensor

An analog compensation circuit was built to implement the velocity sensor given by (2.16). The differentiator was implemented using an op-amp differentiating circuit with a high frequency pole at $p_1 = 1000$ Hz. The sensor velocity, v_{sensor} to primary coil voltage, e_p was then measured experimentally and compared to the actual velocity measured by the velocity transducer. Figure 2.6. shows the measured velocity compared with the modeled and measured sensor response.
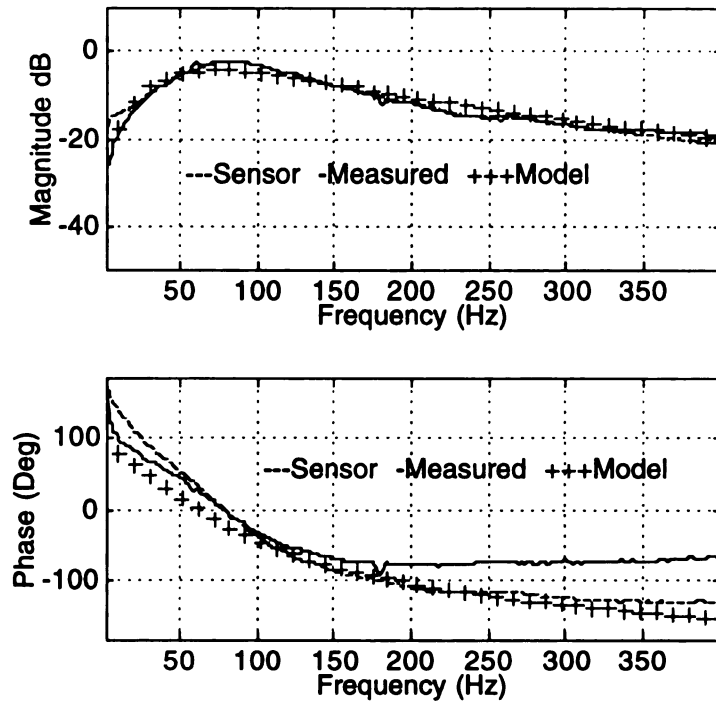
Figure 2.6. Comparison of Velocity Sensor and Measured Velocity

The velocity sensor gives good results below approximately 200 Hz.

There is with less than 2 dB magnitude and 20 degrees phase difference in this

frequency band. Minor magnitude and phase variation is exhibited below 20

Hz, and a significant phase variation is exhibited above 200 Hz. These errors

above 200 Hz are due to inductance effects in the speaker which become

significant at higher frequencies causing the degradation of the velocity

sensor response. These results indicate that the effective bandwidth of the

velocity sensor is 0 - 200 Hz.

Velocity Feedback Compensation of Speaker

A proportional controller was applied to the system using the velocity

sensor voltage as the feedback signal. The velocity response was measured

with different values of proportional gain. Figure 2.7 shows the closed-loop

velocity response measured with the velocity transducer with a gain of 1.0, 10

and 50.
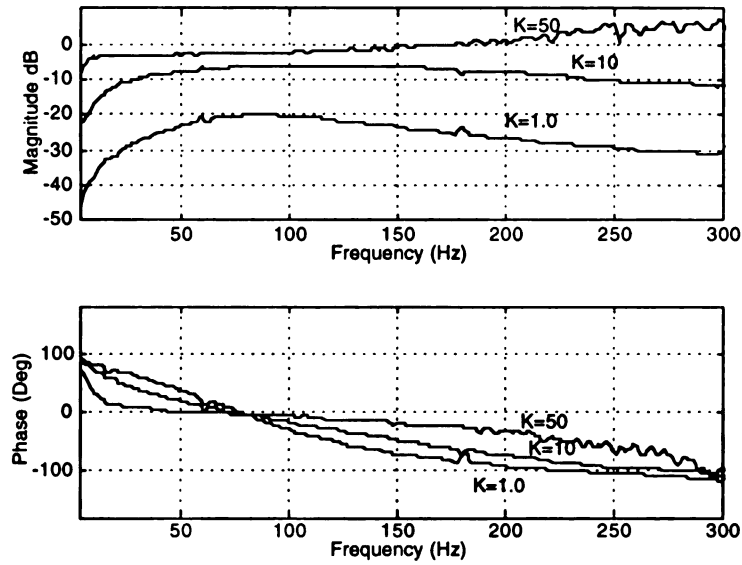
Figure 2.7. Measured Compensated Closed-Loop Velocity Response of
Speaker for Proportional Gain of 1.0, 10, and 50

As predicted, higher gains reduced the magnitude and phase variation.

With a gain of 50, there is less than 5 dB magnitude and 35 degrees of phase

variation from 0 to 200 Hz, compared with 20 dB and 180 degrees magnitude

and phase variation for the uncompensated system. As expected, the

response above 200 Hz is degraded due to the error in the velocity sensor

response.

The results of the compensated speaker using the improved speaker

velocity sensor are comparable and exceed the results obtained using the

previous version of the velocity sensor [Radcliffe et al. 1996]. The largest

magnitude variation shown in Figure 2.7 above 20 Hz is approximately 4 dB, and the largest phase variation is approximately is 45 degrees at 200 Hz. This is an improvement over the previous version of the compensator where the largest variation was 5 dB magnitude and 90 degrees phase with a proportional gain of 50.

The close agreement between the experimental and model results indicate that the model accurately predicts the response of the system. Furthermore, the velocity sensor results demonstrate that the actual velocity of the speaker can be measured through the circuitry of the velocity sensor. Finally, minimization of the magnitude and phase variation in the closed loop response of the speaker indicates that the dynamics of the free-air resonance of the speaker can be reduced through feedback compensation. Together, these results show that the compensated speaker is an effective acoustic actuator with essentially a pure gain from 0 to 200 Hz. This actuator can now be applied to an acoustic system.

3. ACOUSTIC DUCT SYSTEM MODEL

The velocity sensor developed in the previous section has an important feature that was not present in the original velocity sensor. It can predict the speaker response when the velocity is caused by both a primary voltage input and a pressure input. The original velocity sensor [Radcliffe et al. 1996] was based on the assumption that the pressure input was zero, resulting in a sensor that could only predict the velocity if it was caused by a primary voltage input and the pressure on the speaker face was zero. This improvement results in an actuator that compensates for both the free-air resonance of the speaker and any dynamics from a pressure input.

The acoustic duct is a system that exhibits strong dynamics that when coupled with the speaker system will cause large magnitude and phase variations in the speaker response. These effects can then be minimized through feed-back compensation. A numerical model is needed for the acoustic duct before these effects can be demonstrated.

In this section, a model that accurately represents the duct pressure response is developed. System equations are first presented, then they are transformed into state space and transfer function representations. The model is then verified by comparing it with experimental results obtained from an acoustic duct.

System Model

An accurate system model of the acoustic duct is needed for modeling,

analysis. The linear second order wave equation modeling particle

displacement in a hard-walled, one-dimensional duct is [Seto 1971, Doak 1973]

$$\frac{\partial^2 u(x,t)}{\partial t^2} - c^2 \frac{\partial^2 u(x,t)}{\partial x^2} = -\frac{\partial}{\partial x}\left[\frac{\delta(x)P(t)}{\rho}\right] - \sum_{i=1}^{k}[\delta(x-x_i)]\frac{\partial}{\partial t}\left[\frac{M_i(t)}{\rho S}\right] \quad (3.1)$$

where $u(x,t)$ = particle displacement, c = wave speed (m/s), x = spatial

location (m), t = time (s), ρ = density of the medium (kg/m^3), $M_i(t)$ = mass

flow input in the domain (kg/s), x_i = location of mass flow input (m), S =

speaker area driving the mass flow input (m^2), P(t) = pressure excitation at x =

0 (N/m^2), and $\delta(x)$ = the Dirac delta function. The partially reflective

boundary condition at location x = L is the relationship between the spatial

gradient and the time gradient of the particle displacement and is expressed as

[Seto 1971, Spiekerman 1986]

$$\frac{\partial u}{\partial x}(L,t) = -K\left(\frac{1}{c}\right)\frac{\partial u}{\partial t}(L,t); \quad K \neq 0+0i, 1+0i, \infty$$

$$(3.2)$$

where K = complex impedance of the termination end (dimensionless). The

duct end at x = 0 is modeled as a totally reflective end. This boundary

condition is

$$\frac{\partial u}{\partial x}(0,t) = 0 \qquad\qquad (3.3)$$

which corresponds to an open duct end. The acoustic pressure of the system is related to the spatial gradient of the particle displacement by [Seto 1971]

$$P(x,t) = -\rho c^2 \frac{\partial u}{\partial x}(x,t) \qquad\qquad (3.4)$$

The above four equations represent a mathematical model of the duct.

State Space Representation

To derive the state equations used throughout the analysis, separation of variables is applied to the unforced version of (3.1), (3.2) and (3.3). Solving for the separation constant and the eigenfunctions yields [Spiekerman 1990]

$$\lambda_n = \frac{1}{2L}\log_e\left(\frac{1-K}{1+K}\right) - \frac{n\pi i}{L}, \quad n = 0, \pm 1, \pm 2, \dots \qquad (3.5)$$

$$\phi_n(x) = e^{\lambda_n x} + e^{-\lambda_n x} \qquad\qquad (3.6)$$

where λ_n are the natural frequencies and $\phi_n(x)$ are the eigenfunctions of the duct. For a duct with one mass flow rate as the input, the above equations can be manipulated such that the following state space representation is produced:

$$\dot{a}(t) = A_{duct}a(t) + B_{duct}m(t) \tag{3.7}$$

where a(t) = the vector of modal wave amplitudes

A_{duct}= the diagonal matrix $\left[c\lambda_n\right]$

B_{duct} = the matrix $\left\{\left[\dfrac{1}{4c\lambda_n^2 L\rho S}\right]\dfrac{d\phi_n(x_i)}{dx}\right\}$

and m(t) = the mass flow input $\dfrac{\partial M}{\partial t}$

The system output is the pressure at any position in the duct

$$P(x_m,t) = C_{duct}{}^T a(t) \tag{3.8}$$

where $P(x_m,t)$= the pressure in the duct at $x = x_m$,

and C_{duct}= the column vector $\left[-\rho c^2 \dfrac{d\phi_n(x_m)}{dx}\right]$.

Equations (3.7) and (3.8) represent the state space formulation of the acoustic duct with complex impedance, K, on the termination end.

Duct Transfer Function

A velocity to duct pressure transfer function can be computed from the state space representation of the acoustic duct model for the case with one

mass flow input. The transfer function representation will be used for the coupled speaker/duct system model.

The duct transfer function can be computed numerically from

$$G_{duct}(s) = \frac{P_{duct}}{m} = C_{duct}(sI - A_{duct})^{-1}B_{duct} \tag{3.9}$$

where sI is the Laplace variable times an identity matrix and $G_{duct}(s)$ is the speaker velocity to duct pressure transfer function. The mass flow rate, m(t) can be replaced by the speaker face velocity, v_{spkr}, by the relation, $m(t) = S_D v_{spkr}(t)$, where S_D is the speaker area. The transfer function, $G_{duct}(s)$, will have a numerator which consists of a polynomial of order $2*n$ and a denominator of order $2*n+1$, where n is the number of modes in the model.

Duct Model Verification

The duct system model was verified through experimental testing. A duct was assembled, and the system response was measured and compared with the pressure predicted by the model. Figure 3.1 shows the experimental setup with the duct, the driving speaker, the velocity transducer, and the microphone.
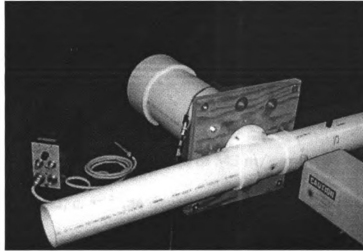
Figure 3.1. Acoustic Duct Experimental Setup with Laser
Velocity Transducer and Microphone

An acoustic duct was constructed from 4-inch diameter PVC pipe. The
duct was 3.43 m long and was fitted with a tee joint so that a speaker could be
mounted in the duct wall, 0.56 m from the open end. A clear window [Hull
et. al. 1993] was added to the tee joint so that the laser velocity transducer
could measure the velocity of the speaker face while maintaining pressure in
the duct, Figure 3.2. Both ends of the duct were left open.
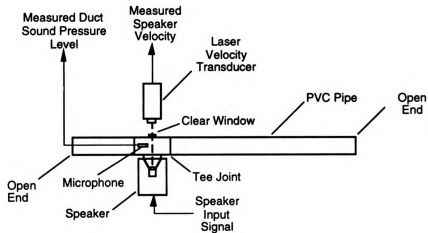
Figure 3.2. Experimental Acoustic Duct System

A half-inch Bruel & Kjaer microphone (model 4155) was placed in the duct at the speaker location. The speaker velocity to duct pressure transfer function was then measured with the signal analyzer with a frequency range from 0 - 200 Hz. The speaker velocity to duct pressure transfer function was also computed using the model. Values of 343 m/s and 1.21 kg/m^3 were used for the speed of sound, c, and the density of air, ρ. The value of the end impedance was varied in the model until the model showed good agreement with the measured response. An end impedance of 0.125+0j was determined to give good model results. Figure 3.3 compares the measured and model velocity to duct pressure transfer function.
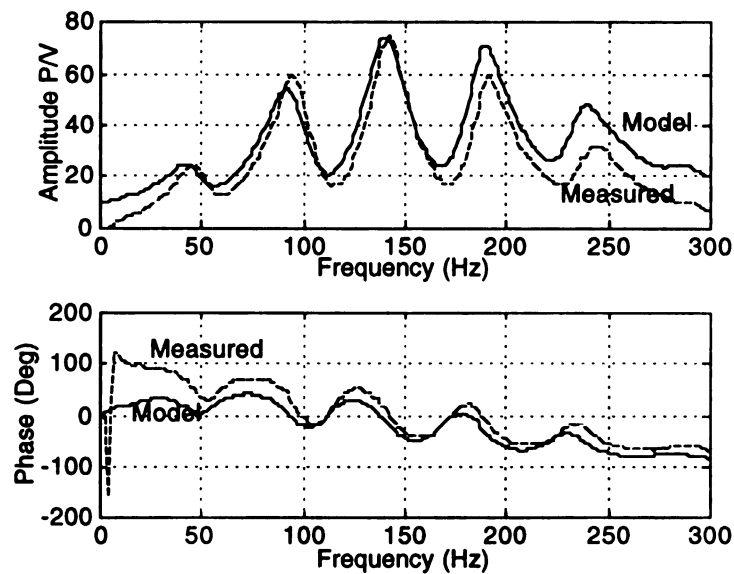
Figure 3.3. Comparison of Model and Measured Velocity to Duct Pressure Transfer Function for Acoustic Duct

The measured response is shown with a solid line, and the model response is shown with a dotted line. Acceptable agreement between the model and the measured response was obtained.

These results verify that the model is accurate and can be used to model the pressure input to the speaker system in the coupled speaker/duct system.

4. COUPLED SPEAKER-DUCT SYSTEM

The coupled speaker/duct system is presented in this chapter. The coupled system is first modeled including the speaker velocity, the velocity sensor, and the closed-loop feedback compensation. The model is then verified by comparing it with experimental results obtained from the coupled speaker/duct setup.

Modeling of Coupled Speaker-Duct System

In the previous discussions both the dynamics of a speaker and a duct were modeled separately. The model of the speaker assumed that the speaker face was exposed to atmospheric pressure. This implied that the speaker velocity was only affected by the primary speaker voltage. The model of the duct gave the pressure at a point in the duct given a velocity input.

These two systems can be coupled by allowing the velocity output of the speaker to be the input to the duct and the pressure output of the duct to be the input to the speaker. The velocity of the speaker face is then no longer affected only by the primary speaker voltage but also by the pressure generated in the duct, which must be determined from the coupled dynamics of the two systems.

The model of the speaker dynamics is given by (2.1) and (2.3) rewritten here in general form

$$\dot{x}_{spkr}(t) = A_{spkr}x_{spkr}(t) + B_{spkr}u_{spkr}(t) + D_{spkr}w_{spkr}(t) \tag{4.1}$$

$$y_{spkr}(t) = C_{spkr}x_{spkr}(t) \tag{4.2}$$

where u_{spkr} is the speaker face pressure, w_{spkr} is the speaker voltage, and y_{spkr} is the speaker velocity. The model of the acoustic duct dynamics is given by (3.9) rewritten here in the general form

$$\dot{x}_{duct}(t) = A_{duct}x_{duct}(t) + B_{duct}u_{duct}(t) \tag{4.3}$$

$$y_{duct}(t) = C_{duct}x_{duct}(t) \tag{4.4}$$

where u_{duct} is the duct input velocity and y_{duct} is the duct pressure.

When the speaker face has constant pressure, the transfer function G(s) can then be determined by dropping the term involving P_{duct} and solving for V_{spkr}/E_p. For the coupled system, however, the output from the speaker, v_{spkr} becomes the input to the duct and the output to the duct, P becomes the input to the speaker. Figure 4.1 illustrates the coupled system.

Speaker

w_{spkr}

Speaker Primary Voltage

$$\dot{x}_{spkr}(t) = A_{spkr}x_{spkr}(t) + B_{spkr}u_{spkr}(t) + D_{spkr}w_{spkr}(t)$$

$$y_{spkr}(t) = C_{spkr}x_{spkr}(t)$$

$u_{duct}(t) = y_{spkr}(t)$

Speaker Face Pressure

Speaker Velocity

$y_{duct}(t) = u_{spkr}(t)$

Duct

$$\dot{x}_{duct}(t) = A_{duct}x_{duct}(t) + B_{duct}u_{duct}(t)$$

$$y_{duct}(t) = C_{duct}x_{duct}(t)$$
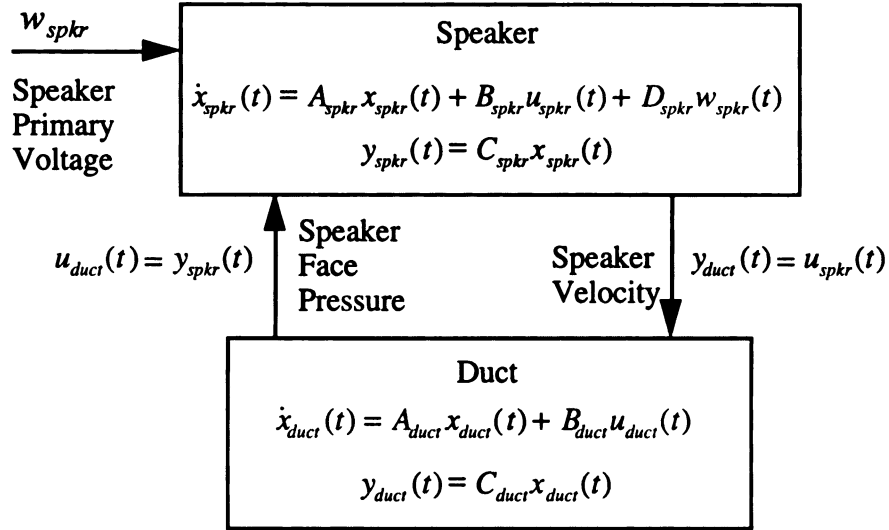
Figure 4.1. Coupled Speaker-Duct System

The coupled system can be modeled by observing that $y_{duct} = u_{spkr}$ and

$u_{duct} = y_{spkr}$.

(4.1) and (4.3) can be rewritten as

$$\dot{x}_{duct}(t) = A_{duct}x_{duct}(t) + B_{duct}C_{spkr}x_{spkr}(t) \tag{4.5}$$

$$\dot{x}_{spkr}(t) = A_{spkr}x_{spkr}(t) + B_{spkr}C_{duct}x_{duct}(t) + D_{spkr}w_{spkr}(t) \tag{4.6}$$

These can then be combined in matrix form as

$$\frac{d}{dt}\begin{pmatrix} x_{duct} \\ x_{spkr} \end{pmatrix} = \begin{bmatrix} A_{duct} & B_{duct}C_{spkr} \\ B_{spkr}C_{duct} & A_{spkr} \end{bmatrix}\begin{pmatrix} x_{duct} \\ x_{spkr} \end{pmatrix} + \begin{bmatrix} 0 \\ D_{spkr} \end{bmatrix}w_{spkr} \tag{4.6}$$

The output to the system is the speaker velocity, given by

$$y_{spkr/duct}(t) = \begin{bmatrix} 0 & C_{spkr} \end{bmatrix} \begin{Bmatrix} x_{duct} \\ x_{spkr} \end{Bmatrix} \qquad (4.8)$$

Equations (4.7) and (4.8) represent the state space equations for the coupled speaker-duct system.

Velocity Sensor

The coupled system (4.7) and (4.8) can be used to model the response of the speaker velocity and the velocity sensor presented in Chapter 2. The speaker velocity, v_{spkr} can be taken from (2.7) to be

$$V_{spkr}(s) = G_{vspkr/ep}(s)E_p(s) + G_{vspkr/P}(s)P(s) \qquad (4.9)$$

The velocity sensor response can be computed by combining the speaker and duct transfer functions (2.7) and (3.9) and eliminating the pressure, P and the secondary coil voltage, e_{bs} terms. The velocity sensor to primary coil voltage is given by

$$V_{sensor}/E_p = \frac{-M_{coil}s}{bl(s+p_1)}\left[G_{ip/ep} + \frac{G_{ip/P}G_{vspkr/ep}G_{duct}}{(1-G_{vspkr/P}G_{duct})} \right] +$$
$$\frac{1}{bl}\left[G_{ebs/ep} + \frac{G_{ebs/P}G_{vspkr/ep}G_{duct}}{(1-G_{vspkr/P}G_{duct})} \right] \qquad (4.10)$$

A complete derivation of (4.10) is given in Appendix F. Equations (4.9) and (4.10) can be used to simulate the speaker velocity and the sensor velocity response of the coupled system.

The feedback compensation strategy proposed in Chapter 2 can be applied to the coupled system. The sensor velocity accounts for the pressure input as well as the primary voltage input, so the closed-loop system should compensate for the dynamics associated with both the speaker and the duct.

Coupled Speaker-Duct Model Verification

The coupled speaker/duct system model was verified through experimental testing. The speaker velocity model was first compared to experimental results, then the velocity sensor was shown to accurately predict the measured velocity. Finally, the velocity sensor was used in feedback compensation. Figure 4.2 shows the coupled speaker/duct experimental setup with the velocity transducer and the compensator.
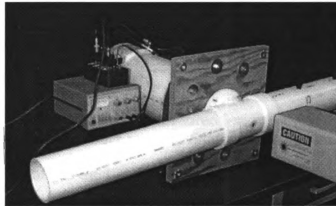
Figure 4.2. Coupled Speaker/Duct Experimental Setup with Laser Velocity Transducer and Velocity Sensor

Speaker Velocity Model

The speaker/duct system was setup as shown in Figure 3.2. The speaker velocity to primary coil voltage transfer function was then measured with the signal analyzer from 0 - 200 Hz. The model given by (4.9) was then used to

compute the model response. Figure 4.3 shows the model response compared to the measured response. The model response is shown by the solid line and the measured response is shown by the dashed line. An end impedance of 0.125+0j was used in the model.

Good agreement was obtained by the model. There is less than 5 dB magnitude difference and 20 degrees and phase difference below 400 Hz.
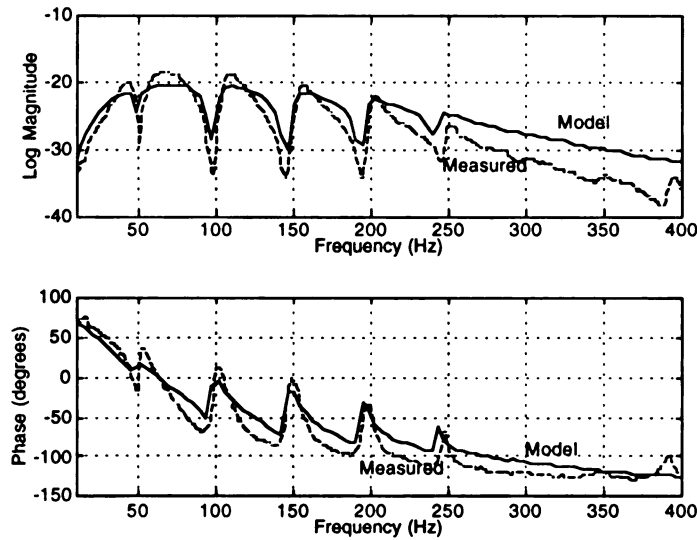
Figure 4.3. Comparison of Measured Frequency Response for
Coupled Duct-Speaker System with Model

The resonances of the duct can clearly be seen in the speaker velocity response. These cause as large as 15 dB and 100 degrees of magnitude and phase variation. The free-air resonance of the speaker is also superimposed on the response. Clearly, the velocity of the speaker is affected by both the speaker and the duct dynamics.

For the application of active noise control of an acoustic duct, the objective is to attenuate the resonances in the duct. Figure 4.2 shows that the

speaker response has the most error exactly where the control effort is needed, at the duct resonance frequencies. The response must be improved if the speaker is to be an effective acoustic actuator.

Velocity Sensor

The velocity sensor presented in Chapter 2 was then applied to the coupled speaker/duct system as show in Figure 4.4. A 2-inch foam plug was placed in the termination end to add damping to the system. An end impedance of 0.6+0.1j was used in the model.
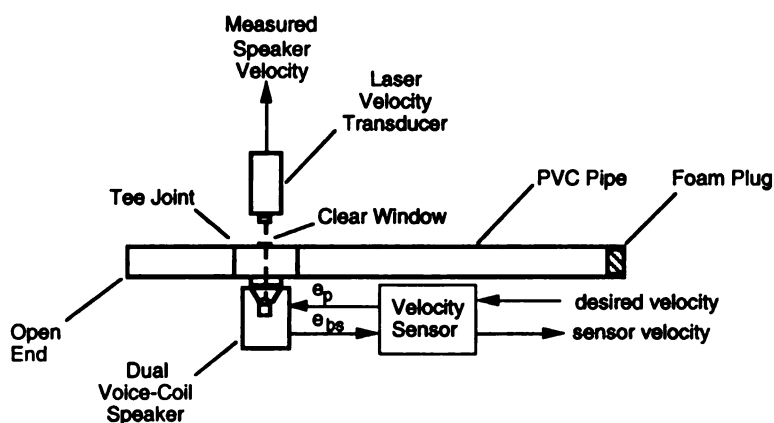
Figure 4.4. Diagram of Velocity Sensor in Speaker/Duct System Implementation

The sensor velocity to desired velocity and measured velocity to desired velocity transfer functions were then measured from 0 - 200 Hz using the signal analyzer. The modeled sensor velocity was also computed with (4.10) using the value of p_1 = 1000 Hz. Figure 4.5 shows good agreement between these three signals.
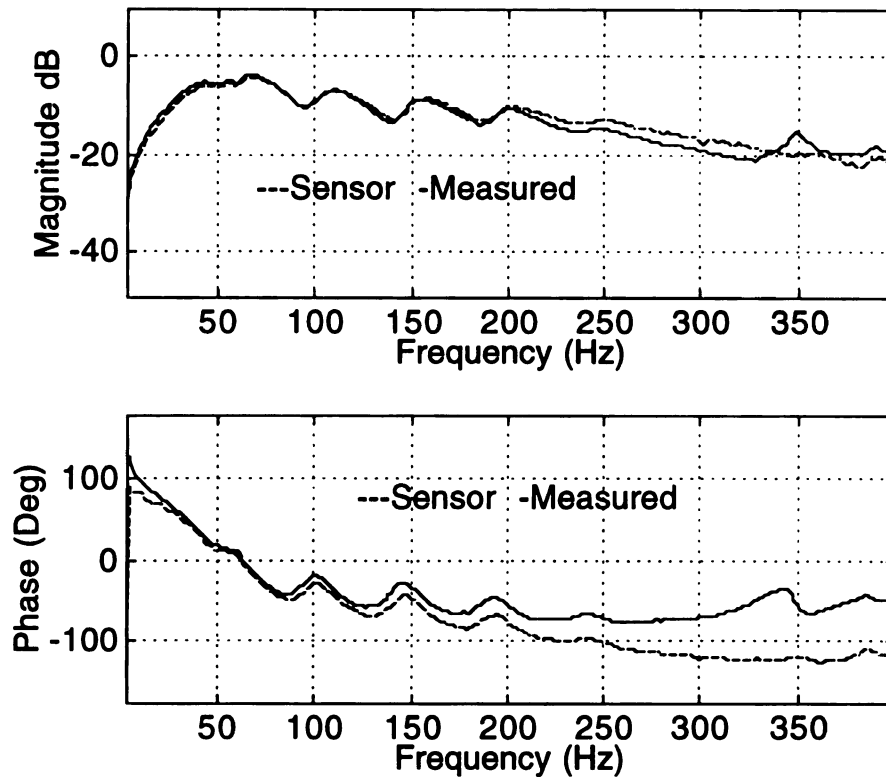
Figure 4.5. Comparison of Measured, Modeled and Sensor Model Speaker
Velocity for Coupled Speaker/Duct System

Figure 4.5 shows that the good agreement between the measured velocity

and the velocity sensor below approximately 200 Hz. There is less than 4 dB

magnitude and 20 degrees phase difference between the two responses. There

is significant phase error above 200 Hz which was seen with the experimental

results for the speaker only. Similarly, this error is attributed to the

inductance effects in the speaker which become significant at high

frequencies.

Velocity Feedback Compensation of Speaker

The velocity feedback compensation strategy presented in Chapter 2 was

then applied to the coupled speaker/duct system. The proportional gain, K_p,

was varied from 0 to 100; and the measured velocity to desired velocity

transfer function was measured from 0 - 200 Hz using the signal analyzer.

Figure 4.6 shows that the measured speaker velocity response approached the

desired velocity as the gain was increased. The noticeable deviation between

the velocity sensor and the measured velocity may contribute to the 45 degree

phase error above 100 Hz in the closed-loop system.
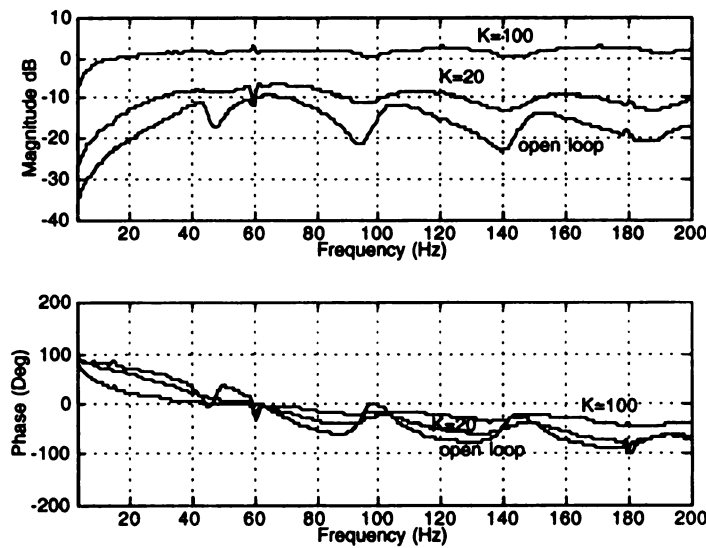
Figure 4.6. Comparison of Closed-Loop Speaker Velocity to Primary Speaker
Voltage Frequency Response for Open Loop and
Proportional Gains of 10, 20, and 100

The magnitude and phase variations exhibited in open-loop have been

minimized. The effect of the duct resonances and the free-air resonance of

the speaker are significantly reduced. With a value of K_p = 100 there is less

than 5 dB and 45 degrees magnitude and phase variation compared with 30

dB and 180 degrees in the uncompensated system. The compensated speaker

velocity is independent from the speaker and duct dynamics. This response is

ideal for an acoustic actuator.

5. CONCLUSIONS

Velocity feedback compensation for minimizing the magnitude and phase variations in the velocity frequency response of a dual-voice coil speaker coupled with an acoustic duct is presented in this work. The feedback compensation uses a proportional controller to drive the speaker through the primary speaker coil. The speaker cone velocity sensing is accomplished by a new velocity sensor designed using the bond graph model of a speaker. It uses a combination of speaker cone motion induced secondary coil voltage and primary coil current.

The speaker velocity feedback compensation is experimentally shown to reduce speaker velocity magnitude and phase variations. The compensated speaker has variations less then 5 dB and 20 degrees in magnitude and phase over a 0 - 200 Hz bandwidth compared to 30 dB and 180 degrees variation in the uncompensated speaker. This advance makes the speaker an ideal actuator in systems with strong coupling between the plant and the actuator, as in active noise control of an acoustic duct.

APPENDIX

APPENDIX A

DERIVATION OF SPEAKER MODEL STATE EQUATIONS

The electromagnetic speaker is a system involving mechanical, electrical and magnetic energy domains. This class of problem is well suited to modeling using the Bond Graph technique [Karnopp & Rosenberg 1983]. Figure A.1 shows the bond graph diagram of the dual voice-coil speaker system.
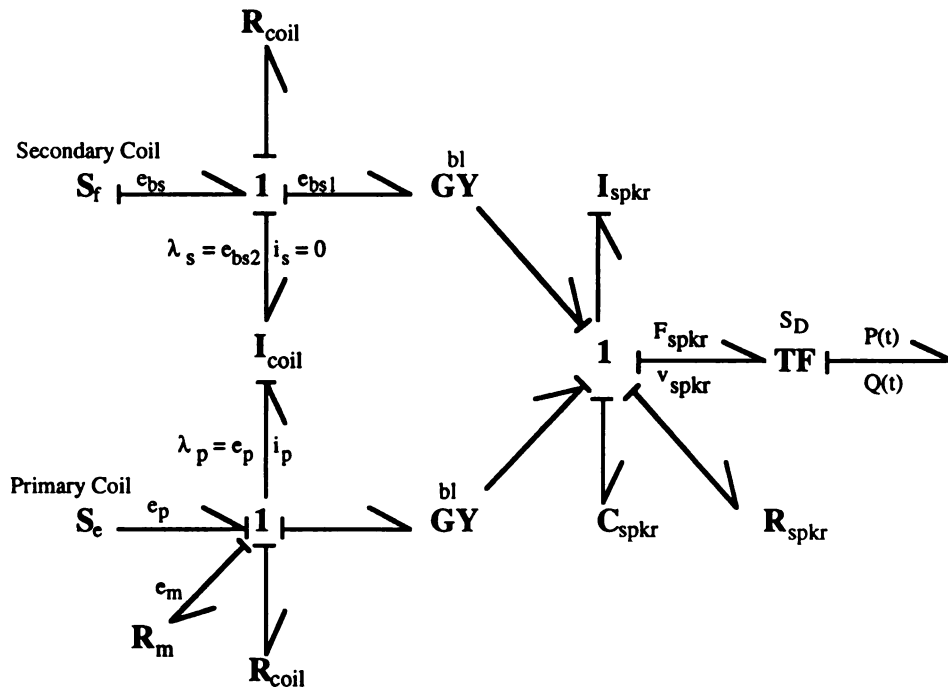

Figure A.1. Bond Graph of Dual Voice-Coil Speaker System

The Bond Graph arrows represent power flow from the electrical voltage, S_e, applied at the primary coil through the model's elements. Power

is dissipated in resistive elements R_{coil}, R_m and R_{spkr}, and transformed both from electrical to mechanical power in the 'GY' element and from mechanical to acoustic power in the 'TF' element. Power is stored as kinetic energy in the 'I' elements and as potential energy in the 'C' elements. The open circuit on the secondary coil is represented by a secondary coil current, i_s =0 imposed by the source of flow, S_f.

The energy variables in the bond graph model include coil flux linkages, λ_p and λ_s, speaker cone displacement x_{spkr} and speaker cone velocity, v_{spkr}. A linear approximation is used to relate the flux linkages, λ_p and λ_s, of the multiport I_{coil} field to the port currents i_p and i_s in the primary and secondary coils.

$$\lambda = Ii \tag{A.1}$$

where, $I = \begin{bmatrix} I_{coil,p} & M_{coil,p} \\ M_{coil,s} & I_{coil,s} \end{bmatrix}$ is the inductance matrix, $i = \begin{pmatrix} i_p \\ i_s \end{pmatrix}$ is the vector of port currents and $\lambda = \begin{pmatrix} \lambda_p \\ \lambda_s \end{pmatrix}$ is the vector of coil flux linkages. $I_{coil,p}$ and $I_{coil,s}$ in the inductance matrix are the self inductances of the primary and secondary coils, and $M_{coil,p}$ and $M_{coil,s}$ are the mutual inductances between primary and secondary coils. The self and mutual inductance terms in the inductance matrix are equal for audio voice-coil speakers because the coils are designed to be identical in construction.

$$M_{coil,p} = M_{coil,s} = M_{coil} \tag{A.2}$$

$$I_{coil,p} = I_{coil,s} = I_{coil} \tag{A.3}$$

For this application, the secondary coil is always an open circuit. Therefore the current in the secondary coil, $i_s(t)=0$. With this, the relation between flux linkages, λ_p and λ_s and primary current, $i_p(t)$ is given by

$$\lambda_p = I_{coil} i_p \tag{A.4}$$

$$\lambda_s = M_{coil} i_p \tag{A.5}$$

The state equations for the speaker model can be written from the bond graph in state space form by choosing energy variables as state variables and appropriate input and output variables as

$$\dot{x}(t) = A_{spkr} x(t) + B_{spkr} u_{spkr}(t) \tag{A.6}$$

where

$$A_{spkr} = \begin{bmatrix} 0 & 1 & 0 \\ \dfrac{-1}{C_{spkr} I_{spkr}} & \dfrac{-R_{spkr}}{I_{spkr}} & \dfrac{bl}{(I_{spkr} I_{coil})} \\ 0 & -bl & \dfrac{-(R_{coil} + R_m)}{I_{coil}} \end{bmatrix}, \; B_{spkr} = \begin{bmatrix} 0 & 0 \\ 0 & \dfrac{-S_D}{I_{spkr}} \\ 1 & 0 \end{bmatrix} \tag{A.7}$$

The state variables are $x_{spkr} = \begin{pmatrix} x_{spkr} \\ v_{spkr} \\ \lambda_p \end{pmatrix}$, speaker face displacement x_{spkr}, speaker

face velocity, v_{spkr} and primary coil flux λ_p, and the input variables are $u_{spkr} = \begin{pmatrix} e_p \\ P \end{pmatrix}$, speaker primary coil voltage, e_p, and speaker face pressure, P.

The output variables can be arranged in state equation format as,

$$y_{spkr} = C_{spkr} x_{spkr} + D_{spkr} u_{spkr} \tag{A.8}$$

where

$$C_{spkr} = \begin{bmatrix} 0 & bl\left(1 - \dfrac{M_{coil}}{I_{coil}}\right) & -\dfrac{M_{coil}}{I_{coil}^2}(R_{coil} + R_m) \\ 0 & 0 & \dfrac{1}{I_{coil}} \\ 0 & 1 & 0 \end{bmatrix}, \; D_{spkr} = \begin{bmatrix} \dfrac{M_c}{I_c} & 0 \\ 0 & 0 \\ 0 & 0 \end{bmatrix} \tag{A.9}$$

The output variables, $y_{spkr} = \begin{pmatrix} e_{bs} \\ i_p \\ v_{spkr} \end{pmatrix}$ are speaker secondary coil voltage, $e_{bs}(t)$,

speaker drive current in the primary coil, $i_p(t)$, and speaker face velocity, v_{spkr}.

The voltage, $e_{bs}(t)$, introduced in the secondary speaker coil is obtained from the bond graph model by summing the voltages across the 1-junction on the secondary coil side of the I_{coil} element. These voltages include the voltage, $e_{bs1}(t)$, due to the mechanical motion of the speaker cone and the voltage, $e_{bs2}(t)$ due to the mutual inductance, M_{coil}, between the coils.

$$e_{bs}(t) = e_{bs1}(t) + e_{bs2}(t) \tag{A.10}$$

The voltage, $e_{bs1}(t)$, introduced due to the mechanical motion of the speaker cone is linearly proportional to the speaker cone velocity, v_{spkr}

$$e_{bs1}(t) = bl \, v_{spkr}(t) \tag{A.11}$$

The voltage, $e_{bs2}(t)$, in the secondary speaker coil can be written from the constitutive relation of the coils by noting that the secondary coil current, $i_s = 0$ due to the open circuit condition on the secondary coil.

$$e_{bs2}(t) = \dot{\lambda}_s = M_{coil} \frac{di_p(t)}{dt} \tag{A.12}$$

Therefore, the voltage, $e_{bs}(t)$, introduced in the secondary speaker coil is

$$e_{bs}(t) = bl \, v_{spkr} + M_{coil} \frac{di_p(t)}{dt} \tag{A.13}$$

The primary coil current, $i_p(t)$ can be replaced by λ_p / I_{coil} yielding

$$e_{bs}(t) = bl \, v_{spkr} + \frac{M_{coil}}{I_{coil}} \frac{d\lambda_p(t)}{dt} \tag{A.14}$$

The term $\dfrac{d\lambda_p(t)}{dt}$ can be replaced with row 2 from (A.7) giving,

$$e_{bs}(t) = bl\left(1 - \frac{M_c}{I_c}\right)v_s(t) - \frac{M_c}{I_c^2}(R_c + R_m)\lambda_p(t) + \frac{M_c}{I_c}e_p(t) \tag{A.15}$$

The output equation can now be written for the output variables, secondary coil voltage, $e_{bs}(t)$, primary coil current, $i_p(t)$ and speaker velocity, $v_{spkr}(t)$ in terms of the state variables, speaker displacement, x_{spkr}, speaker velocity, v_{spkr}, and primary coil flux linkage, λ_p, and the input variables, primary coil voltage, e_p, and pressure, P as,

$$
\begin{pmatrix} e_{bs} \\ i_p \\ v_{spkr} \end{pmatrix} = \begin{bmatrix} 0 & bl\left(1 - \dfrac{M_{coil}}{I_{coil}}\right) & -\dfrac{M_{coil}}{I_{coil}^2}(R_{coil} + R_m) \\ 0 & 0 & \dfrac{1}{I_{coil}} \\ 0 & 1 & 0 \end{bmatrix} \begin{pmatrix} x_{spkr} \\ v_{spkr} \\ \lambda_p \end{pmatrix} + \begin{bmatrix} \dfrac{M_c}{I_c} & 0 \\ 0 & 0 \\ 0 & 0 \end{bmatrix} \begin{pmatrix} e_p \\ P \end{pmatrix} \quad (A.16)
$$

Equations (A.7) and (A.16) define the model of a dual voice-coil speaker.

APPENDIX B

SPEAKER PARAMETER IDENTIFICATION

The physical parameters of the speaker were determined using a methodology given by [Radcliffe, Gogate, 1992].

1. The speaker compliance, C_{spkr} is given by staticly loading the speaker face with a digital force meter and measuring displacement and determining slope from force vs. displacement graph.

Table B.1. Speaker Compliance Data

Displacement (m)	Force (N)
0	0
0.002	3.1392
0.004	7.7499
0.006	14.96025
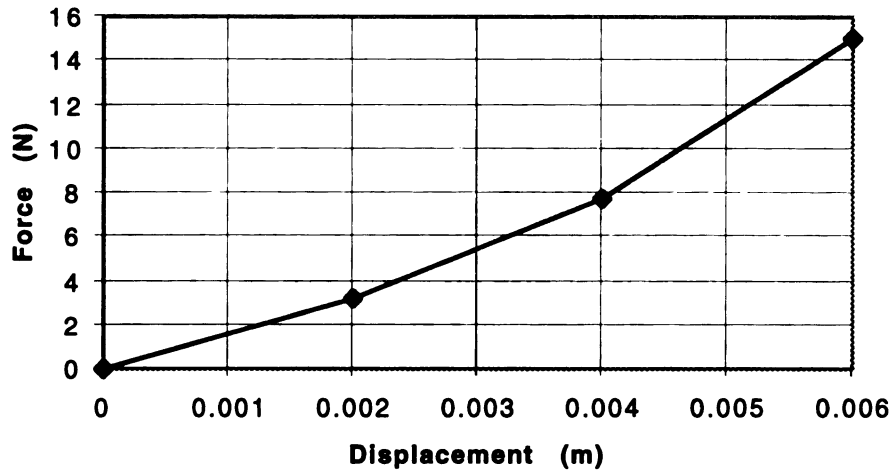
Figure B.1. Force Vs Displacement Graph for Speaker

Cspkr = 0.000868 m/N25

2. The speaker resonant frequency f_n. is determined from the frequency response of speaker velocity to primary coil voltage, Figure B.2.
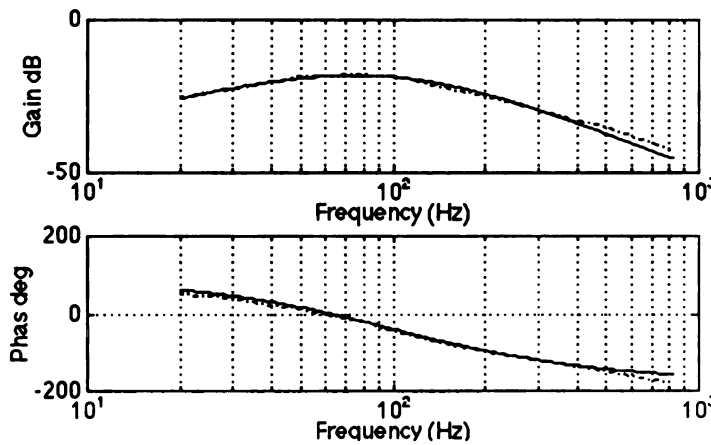
Figure B.2. Frequency Response of Speaker Face Velocity to Primary Coil Voltage

$f_n = 62\,Hz$

3. The damping factor ζ is determined from the half power points on Figure B.2 and the quality factor, Q.

resonance frequency $f_n = 62\,Hz$

half power frequencies   f1 = 36 Hz, 125 Hz

Quality Factor, Q is given by,

$$Q = \frac{f_n}{f_2 - f_1} = \frac{62}{125 - 36} = 0.697 \qquad \text{(B-1)}$$

Damping ratio ζ is given by,

$$\zeta = \frac{1}{2Q} = \frac{1}{2(0.696)} = 0.718 \qquad \text{(B-2)}$$

4.   The primary and secondary coil resistance is obtained by measuring each resistance with an ohm meter.

$$R_{coil} = 4.875 \text{ ohms}$$

5.   The speaker inertia, Ispkr is determined from

$$I_{spkr} = \frac{1}{C_{spkr}(2\pi f_n)^2} = \frac{1}{(0.000868m/N)(389 rad/s)^2} = 0.0076 kg \qquad \text{(B-3)}$$

6.   The electromagnetic coupling factor, bl is obtained from

$$bl = 10^{(M/20)} \frac{I_{spkr} R_{coil} \left[\left(\omega_a^2 - \omega_1^2 \right)^2 + 4(\zeta\omega_1\omega_n)^2 \right]}{\sqrt{\left[\omega_1 \left(\omega_a^2 - \omega_1^2 \right) \right]^2 + \left[2\zeta\omega_1^2\omega_n \right]^2}} \qquad \text{(B-4)}$$

where M is the magnitude of the frequency response at a frequency ω_1. Using M=-20 dB and ω_n= 251.33 rad/s,

$$bl = 2.4566 \text{ N/A}$$

7.   The equivalent speaker area is given by 87% of the advertised cone area as,

$$S_D = 0.87 \left(\frac{\pi}{4} D \right)^2 = 0.87(0.0153m^2) = 0.0133m^2 \qquad \text{(B-5)}$$

where the advertised diameter, D is 0.140m (5.5 inches).

8.   The speaker viscous friction constant, R_{spkr} is given by

$$R_{spkr} = \sqrt{\frac{I_{spkr}}{C_{spkr}}} \frac{1}{Q} - \frac{bl^2}{R_{coil}} = 3.745 \text{ N sec}/m \qquad \text{(B-6)}$$

A summary of the speaker parameters is given blow.

Table B.2. Speaker System Physical Parameters

Parameter	Symbol	Value
mechanical inertia	I_{spkr}	0.0076 Kg
mechanical compliance	C_{spkr}	0.000868 m/N
viscous friction	R_{spkr}	3.745 N sec/m
electromagnetic coupling factor	bl	2.45 N/A
coil resistance	R_{coil}	4.875 ohm
equivalent speaker area	S_D	0.0133m^2

APPENDIX C

DERIVATION OF SPEAKER MODEL TRANSFER FUNCTIONS

The transfer function matrix for the speaker model can be determined from (2.1) and (2.3). The speaker model includes two inputs and three outputs, resulting in a transfer function matrix of dimension 3x2. The steady-state output of the system is given by [Rough 1996]

$$Y(s) = \left[C(sI - A)^{-1}B + D \right] U(s) \tag{C.1}$$

where A is the state matrix, B is the input matrix, C is the output matrix, D is the direct feed-through matrix, 'sI' is the Laplace variable multiplied by an identity matrix, U(s) and Y(s) is are the input and output vectors in the Laplace domain.

The transfer function matrix is defined by

$$G(s) = C(sI - A)^{-1}B + D \tag{C.2}$$

The state equation matrices for the speaker model are

$$A_{spkr} = \begin{bmatrix} 0 & 1 & 0 \\ \dfrac{-1}{C_{spkr}I_{spkr}} & \dfrac{-R_{spkr}}{I_{spkr}} & \dfrac{bl}{(I_{spkr}I_{coil})} \\ 0 & -bl & \dfrac{-(R_{coil} + R_m)}{I_{coil}} \end{bmatrix}, \quad B_{spkr} = \begin{bmatrix} 0 & 0 \\ 0 & \dfrac{-S_D}{I_{spkr}} \\ 1 & 0 \end{bmatrix}$$

$$C_{spkr} = \begin{bmatrix} 0 & bl\left(1 - \dfrac{M_{coil}}{I_{coil}}\right) & -\dfrac{M_{coil}}{I_{coil}^2}(R_{coil} + R_m) \\ 0 & 0 & \dfrac{1}{I_{coil}} \\ 0 & 1 & 0 \end{bmatrix}, \quad D_{spkr} = \begin{bmatrix} \dfrac{M_c}{I_c} & 0 \\ 0 & 0 \\ 0 & 0 \end{bmatrix}$$

Computing (sI-A) gives

$$(sI - A) = \begin{bmatrix} s & -1 & 0 \\ \dfrac{1}{C_{spkr}I_{spkr}} & s + \dfrac{R_{spkr}}{I_{spkr}} & \dfrac{-bl}{(I_{spkr}I_{coil})} \\ 0 & bl & s + \dfrac{R_{coil}}{I_{coil}} \end{bmatrix} \qquad (C.3)$$

Computing C(sI-A)⁻¹B yields

$$\begin{pmatrix} e_{bs}(s) \\ i_p(s) \\ v_{spkr}(s) \end{pmatrix} = \begin{bmatrix} G_{ebs/ep} & G_{ebs/P} \\ G_{ip/ep} & G_{ip/P} \\ G_{vspkr/ep} & G_{vspkr/P} \end{bmatrix} \begin{pmatrix} e_p(s) \\ P(s) \end{pmatrix} \qquad (C.4)$$

where each element in the transfer function matrix G(s) is given by

$$G_{ebs/ep} = \left[(C_{spkr}I_{spkr}M_{coil})s^3 + (C_{spkr}R_{spkr}M_{coil})s^2 + (bl^2C_{spkr} + M_{coil})s\right] \Big/ G_{den} \qquad (C.5)$$

$$G_{ep/ep} = \left[(C_{spkr}I_{spkr})s^2 + (C_{spkr}R_{spkr})s + 1\right] \Big/ G_{den} \qquad (C.6)$$

$$G_{vspkr/ep} = \left[(bl\, C_{spkr})s\right] \Big/ G_{den} \qquad (C.7)$$

$$G_{ebs/P} = \left[-bl\, C_{spkr}S_D\left[(I_{coil} - M_{coil})s^2 + R_{coil}s\right]\right] \Big/ G_{den} \qquad (C.8)$$

$$G_{ip/P} = \left[(bl\, S_D C_{spkr})s\right] \Big/ G_{den} \qquad (C.9)$$

$$G_{vspkr/P} = \left[-S_D C_{spkr}\left[I_{coil}s^2 + R_{coil}s\right]\right] \Big/ G_{den} \qquad (C.10)$$

and the denominator of the G(s) matrix is given as,

$$G_{den} = (C_{spkr}I_{spkr}I_{coil})s^3 + (C_{spkr}I_{spkr}R_{coil} + C_{spkr}I_{coil}R_{spkr})s^2 +$$
$$(bl^2C_{spkr} + I_{coil} + C_{spkr}R_{coil}R_{spkr})s + R_{coil}$$

(C.11)

APPENDIX D

COMPENSATOR CIRCUIT IMPLEMENTATION

The speaker compensation is implemented with an analog circuit which includes the velocity sensor and the proportional controller.

The velocity sensor equation is given by,

$$v_{spkr}(s) = H_{bs}E_{bs}(s) - H_p(s)I_p(s) \tag{D.1}$$
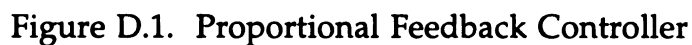
where $H_{bs} = 1/bl$ and $H_p(s) = sM_{coil}/bl$.

The secondary coil voltage, e_{bs} can be measured directly from the speaker coil, the primary coil current, i_p can be determined from the voltage across the resistor R_{m_r}. H_{bs} is a pure gain $(1/bl)$, and the term $H_p(s)$ is a differentiator transfer function because it contains an 's' in the numerator. Such a transfer function can not be realized exactly but an approximation $\hat{H}_p(s)$ can be used, where

$$\hat{H}_p(s) = \frac{M_{coil}}{bl}\left(\frac{s}{s+p_1}\right) \tag{D.2}$$

where p_1 is a pole location selected such that $\hat{H}_p(s)$ approximates $H_p(s)$ over the controller bandwidth.

Feedback compensation can now be implemented using the signal from the velocity sensor to compute the error between the desired velocity and the sensor velocity and a proportional controller to drive the speaker

velocity to the desired velocity. The proportional controller in block diagram form is given in Figure D.1.

Figure D.1. Proportional Feedback Controller

A circuit diagram of the compensation circuit used in the experimental portion of this study is given here.

Figure D.2. Speaker Compensation Circuit Diagram

An external amplifier was used to implement the gain K_p. Figure D.3 shows the overall arrangement of the compensated speaker components.
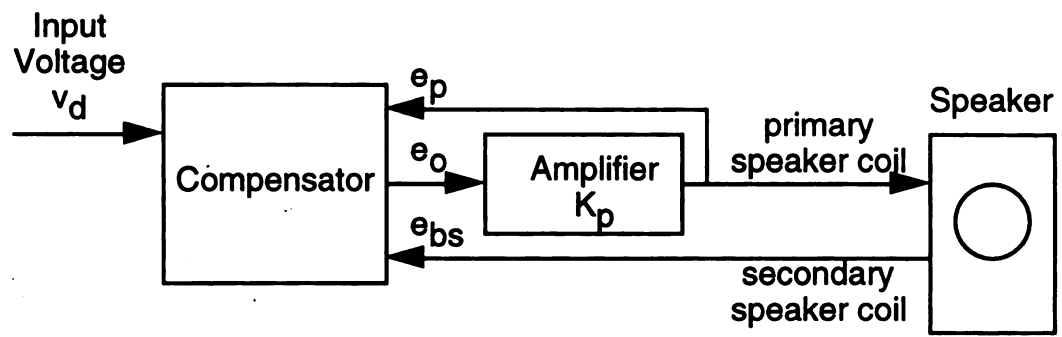
Figure D.3. Overall Arrangement of Compensated Speaker Components

APPENDIX E

ACOUSTIC DUCT STATE EQUATION COMPUTATION ALGORITHM

The acoustic duct state equations were computed from the equations given in Section 3 using a numerical algorithm in the Matlab software programming environment. The algorithm, given blow takes the number of modes to be generated and returns the state equation matrices, A, B, C, and D.

Matlab Program for Computing Acoustic Duct State Equations

```
function [A,B,C,D,N]=genstsp(N)
%M-File to generate state space matricies for acoustic duct
%Input number of modes N to include in model

%Define Variables
L=140*.0254;                    %Length of Duct 2.1336m,118in
K=0.125+0*i;                    %Impedance of Duct End 0.1268+0.0*i
S=0.009;%.25*pi*(6*.0254)^2     %Speaker area m^2
xm=22*.0254;                    %Location of measurement in duct 0.7874
xi=22*.0254;                    %Location of disturbance input
c=343;                          %Wave speed 343 m/s
ro=1.21;                        %Density of medium air 1.21 kg/m^3

for n= -N:N
    count=n+N+1;
      Ln(count)=1/2/L*log((1-K)/(1+K))-n*pi*i/L;
      pdotm(count)=Ln(count)*(exp(Ln(count)*xm)-exp(-Ln(count)*xm));
      pdoti(count)=Ln(count)*(exp(Ln(count)*xi)-exp(-Ln(count)*xi));
      B(count,1)=pdoti(count)/(4*c*(Ln(count)^2)*L*ro*S); %controller
      Dn(count,1)=-1/(2*c*L*ro*Ln(count));   %disturbance
      C(count,1)=-ro*c*c*pdotm(count);
end

A=diag(c*Ln);
D=[0];
end
```

APPENDIX F

COUPLED SPEAKER/DUCT VELOCITY SENSOR TRANSFER FUNCTION

The coupled system can be used to model the response of the speaker velocity and the velocity sensor presented in Chapter 2. The speaker velocity, V_{spkr} is given by

$$\begin{pmatrix} E_{bs}(s) \\ I_p(s) \\ V_{spkr}(s) \end{pmatrix} = \begin{bmatrix} G_{ebs/ep} & G_{ebs/P} \\ G_{ip/ep} & G_{ip/P} \\ G_{vspkr/ep} & G_{vspkr/P} \end{bmatrix} \begin{pmatrix} E_p(s) \\ P(s) \end{pmatrix} \tag{F.1}$$

as

$$V_{spkr}(s) = G_{vspkr/ep}(s)E_p(s) + G_{vspkr/P}(s)P(s) \tag{F.2}$$

The velocity sensor response can be computed by combining the speaker and duct transfer functions and eliminating the pressure, P and secondary coil voltage, E_{bs}. The duct pressure to speaker velocity transfer function is given by

$$P_{duct}\Big/V_{duct} = G_{duct} \tag{F.3}$$

The pressure can be eliminate from (F.2) by substituting (F.3) which gives

$$V_{spkr}(s) = G_{vspkr/ep}(s)E_p(s) + G_{vspkr/P}(s)G_{duct}(s)V_{spkr}(s) \tag{F.4}$$

which can be solved for the transfer function of speaker velocity to primary speaker voltage as

$$V_{spkr} \Big/ E_p = \frac{G_{vspkr/ep}}{\left(1 - G_{vspkr/P}G_{duct}\right)} \qquad (F.5)$$

The secondary speaker voltage was given by (F.1). The pressure, P can be eliminated from (F.1) using (F.3), giving

$$E_{bs}(s) = G_{ebs/ep}E_P + G_{ebs/P}G_{duct}V_{spkr} \qquad (F.6)$$

The velocity can be eliminated from (F.6) using (F.5) giving the secondary speaker voltage to primary speaker voltage transfer function as,

$$E_{bs}/E_P = G_{ebs/ep} + \left[\frac{G_{ebs/P}G_{vspkr/ep}G_{duct}}{(1 - G_{vspkr/P}G_{duct})}\right] \qquad (F.7)$$

The primary speaker current, I_p is given by (F.1). The pressure and velocity can be eliminated as before, giving,

$$I_P/E_P = G_{ip/ep} + \left[\frac{G_{ip/P}G_{vspkr/ep}G_{duct}}{(1 - G_{vspkr/P}G_{duct})}\right] \qquad (F.8)$$

The velocity sensor equation is given by

$$v_{spkr}(s) = H_{bs}E_{bs}(s) - H_p(s)I_p(s) \qquad (F.9)$$

where $H_{bs} = 1/bl$ and $H_p(s) = sM_{coil}/bl$. (F.5) and (F.8) can be substituted into (F.9) to give the sensor velocity to primary speaker voltage transfer function as,

$$V_{sensor}/E_p = \frac{-M_{coil}s}{bl(s+p_1)}\left[G_{ip/ep} + \frac{G_{ip/P}G_{vspkr/ep}G_{duct}}{(1 - G_{vspkr/P}G_{duct})}\right] + $$
$$\frac{1}{bl}\left[G_{ebs/ep} + \frac{G_{ebs/P}G_{vspkr/ep}G_{duct}}{(1 - G_{vspkr/P}G_{duct})}\right] \qquad (F.10)$$

These equations, (F.2) and (F.10) can be used to simulate the speaker velocity and the sensor velocity response of the coupled system.

LIST OF REFERENCES

LIST OF REFERENCES

Bradley, P., *"Active Assault on Cabin Noise"*, Commercial Aviation vol 77, September, 1995, 6 pp.

Warner, J., *"Active Noise Control in an Off-Road Vehicle Cab"* Noise and Vibrations Worldwide, vol 26 n, 7 July, 1995.

General Motors 1994, Report #.

Hull A. J., Radcliffe C. J. Southward S. C., *"Global Active Noise Control of a One-Dimensional Acoustic Duct Using a Feedback Controller"* Journal of Dynamic Systems, Measurement, and Control, vol 115, September, 1993.

Radcliffe C. J., Gogate, S. D., *"Velocity Feedback Compensation of Electromechanical Speakers for Acoustic Applications"*, International Federation of Automatic Control, Triennial World Congress, July, 1996.

Karnopp, D. C., D. L. Margolis, and R. C. Rosenberg, *"System Dynamics: A Unified Approach"*, New York, John Wiley & Sons, Inc., 1990.

IEEE Standard 219-1975, IEEE Standard Committee of Acoustics, Speech, and Signal Processing Group, *"IEEE Recommended Practice for Loudspeaker Measurements"*, IEEE std. 219-1975.

Rough, W. J., *"Linear System Theory"*, New Jersey, Prentice-Hall, Inc. 1996.

Radcliffe, C. J., Gogate, S. D., *"Identification and Modeling Speaker Dynamics for Acoustic Control Applications"*, ASME Symposium on Active Control of Noise and Vibration, 1992.

Seto, W. W., *"Theory and Problems of Acoustics"*, New York, McGraw-Hill Book Company, 1971.

Doak, P. E., *"Excitation, Transmission and Radiation of Sound From Source Distributions in Hard-Walled Ducts of Finite Length (I): The Effects of Duct Cross-Section Geometry and Source Distributions Space-Time Pattern,"* Journal of Sound and Vibration, v 31, n 1 pp1-72, 1973.

Spiekerman, C. E. and Radcliffe, C. J., *"One-Dimensional Acoustic Response with Mixed Boundary Condition: Separating Total Response into Propagating and Standing Wave Components,"*: Doctoral Dissertation, Michigan State University, 1986.

Hull A. J., Radcliffe C. J., *"State Space Representation of the Nonself-Adjoint Acoustic Duct System,"* Journal of Vibration and Acoustics v 112, October, 1990.